

The Supernova Remnant G296.7–0.9 in X-rays (Research Note)

T. Prinz¹ and W. Becker^{1,2}

¹ Max Planck Institute for extraterrestrial Physics, Giessenbachstrasse, 85741 Garching, Germany
e-mail: tprinz@mpe.mpg.de

² Max-Planck Institut für Radioastronomie, Auf dem Hügel 69, 53121 Bonn, Germany

Received [date] / Accepted [date]

ABSTRACT

Aims. We present a detailed study of the supernova remnant (SNR) G296.7–0.9 in the 0.2–12 keV X-ray band.

Methods. Using data from XMM-Newton we performed a spectro-imaging analysis of G296.7–0.9 in order to deduce the basic parameters of the remnant and to search for evidence of a young neutron star associated with it.

Results. In X-rays the remnant is characterized by a bright arc located in the south-west direction. Its X-ray spectrum can best be described by an absorbed non-equilibrium collisional plasma model with a hydrogen density of $n_H = 1.24^{+0.07}_{-0.05} \times 10^{22} \text{ cm}^{-2}$ and a plasma temperature of $6.2^{+0.9}_{-0.8}$ million Kelvin. The analysis revealed a remnant age of 5800 to 7600 years and a distance of $9.8^{+1.1}_{-0.7}$ kpc. The latter suggests a spatial connection with a close-by HII region. We did not find evidence for a young neutron star associated with the remnant.

Key words. ISM: supernova remnants - ISM: individual objects: G296.7–0.9 - Stars: neutron

1. Introduction

Every year, several hundred supernova (SN) events are observed, representing the end state of stellar evolution in which a core-collapse of a massive star or the thermonuclear disruption of a white dwarf takes place. Most of these events are observed in the optical band by ground based observatories, some in comparing new and old photographic plates. On the other hand, SNe are the most energetic events which we can observe in the universe, making them often as bright as a whole galaxy. Especially the latter property supports observations of SN events up to distances of Gpc (Rodney et al. 2011). At this distance, though, the only information obtainable from them is the characteristic raising and fading of their light as a function of time, i.e. their photometric light-curves, and its spectral evolution, which both allow their classification (Sako et al. 2008).

In our own Galaxy, the rate of observed SNe is small and on average only two per century (Keane & Kramer 2008). Many SNe, though, remain unobserved due to optical light extinction. The last recorded SN in our own Galaxy, the Kepler SN, was observed in AD 1604. Not more than six other SN have been detected in the Galaxy in the past two thousand years (Green & Stephenson 2003). The optical light from the two youngest supernovae known in our Galaxy, G1.9+0.3 and Cas A, were not observed about 100 and 350 years ago (Reynolds et al. 2008; Green & Stephenson 2003).

However, even if the direct light from a SN event was missed, for several nearby ones we have the chance to study at least the light of their remnant, which remains visible in various spectral bands for about 10^5 years. Although the light echo from the SN CAS A has been found recently (Rest et al. 2008), it is one of the few cases so far where the SN light could be studied a few hundred years after the SN event. The most promising way to learn about the evolution of a SN shock front and the feedback

on the evolution of their host galaxy is therefore to study the diffuse emission of supernova remnants.

In the last years several new supernova remnants were detected thanks to the increasing sensitivity of modern X-ray observatories. One of those remnants is G296.7–0.9, which was first detected in X-rays by Schaudel et al. (2002) and later identified to be a SNR by Schaudel (2003) and Robbins et al. (2012). It is a shell-like SNR from which X-ray and radio emission has been detected. In addition, filaments in the infrared and H α band were detected in the near proximity of the source.

A first detailed study of the SNR G296.7–0.9 was presented by Robbins et al. (2012) using ROSAT PSPC data. As this detector had roughly five independent energy channels in the range 0.1–2 keV, the spectral results deduced in their analysis were very limited and suggested that the X-rays were emitted from a thermal plasma. Robbins et al. (2012) therefore were not able to put any constraints with high confidence on the derived spectral parameters. The ROSAT data did not allow to deduce parameters like the age, the expansion velocity of the remnant or its distance.

In this letter we report on an XMM-Newton observation which was targeted to SNR G296.7–0.9. The results of the spatial and spectral analysis of the X-ray data is presented in Section 2. A discussion is given in Section 3 in which we use the inferred spectral parameters of G296.7–0.9 to derive an estimate for the age, the radius, the expansion velocity and the distance. Section 4 provides the concluding summary.

2. X-ray observation and data reduction

G296.7–0.9 was observed for 13.6 ksec on 28 June 2011 with the EPIC cameras (Strüder et al. 2001) on board the X-ray observatory XMM-Newton (ObsID 0675070101). The two MOS and the PN cameras were operated in Full-Frame mode using the medium filter. Part of the observation was taken with the filter

wheel in closed position because the observation was strongly affected by particle background radiation. Therefore, the performed duration was only 4.4 ksec and 5.5 ksec for the PN and MOS1/2 detectors, respectively.

We used the XMM SAS version 11.0.0 to reprocess and reduce the data. Times of high background activity were identified by inspecting the light curves of the MOS1/2 and PN data at energies above 10 keV. After rejecting these times the effective exposures of the PN, MOS1 and MOS2 cameras were 3.7 ksec, 5.1 ksec, and 5.3 ksec, respectively.

We extracted images and exposure maps in the five standard bands of XMM-Newton using all three EPIC instruments. Single and double events were selected from the PN data and single to quadruple events from the MOS data sets.

For the spectral fitting we used the X-Ray Spectral Fitting Package (XSPEC) version 12.7.0u. For the spectral analysis of the extended source emission we restricted the energy range to 0.4–6.0 keV because the count rate detected at higher energies was too sparse for a meaningful spectral analysis. Below 0.4 keV the detector and telescope response is not well established. All given uncertainties in this letter represent the 1σ confidence range for one parameter of interest, unless stated otherwise.

2.1. Spatial analysis

Figure 1 shows the X-ray color image of SNR G296.7–0.9. A bright arc-like structure is clearly detectable in the south-east which is elongated to an elliptically shaped sphere. The center of this ellipse is at $RA_c = 11^h55^m52^s.3 \pm 0^s.7$, $DEC_c = -63^\circ06'29'' \pm 3''$ with a semi major axis of $5'$ and a semi minor axis of $3'.75$.

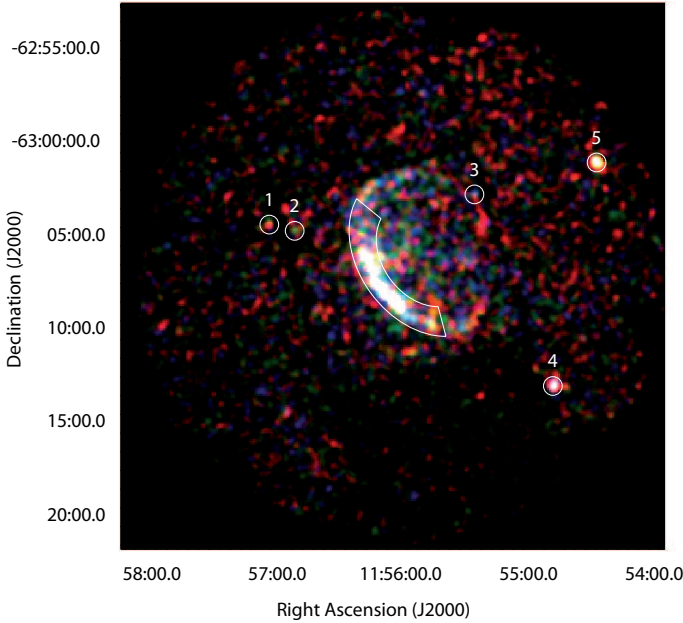


Fig. 1. $29' \times 29'$ XMM-Newton MOS1/2 color image of G296.7–0.9 (red 0.5–0.9 keV, green 0.9–1.3 keV and blue 1.3–2 keV). The superimposed images are binned with $6''$ per pixel and smoothed by a Gaussian kernel of $\sigma = 30''$. The photons detected in the annular sector shown in white were used for spectral analysis of the supernova remnant.

We searched for point sources with a signal-to-noise ratio S/N of at least 3σ in the five standard bands using a sliding box source detection algorithm (SAS tool `edetect_chain`). Five point

sources were detected (see Fig. 1), which all have a $S/N \geq 7\sigma_G$ (σ_G is defined as $\sigma_G = 1 + \sqrt{c_{bg} + 0.75}$, where c_{bg} are the background counts). Their position, positional error and signal-to-noise ratio are listed in Table 1. We cross-correlated the source position with the help of the VizieR online tool¹ by searching for optical counterparts within a square of side length $\approx 6''$ in all available catalogs. This is equal to 3σ , where σ is the error in the source position including the XMM-Newton absolute astrometric accuracy of $\approx 2''$ (r.m.s.).² We found a match for every detected source. These counterparts with their positional displacement from the X-ray source are listed in Table 1.

No source has been detected close to the geometrical center of the supernova remnant. The 3σ upper limit on the count rate of a central compact object is 9×10^{-3} cts/s in the energy range 0.2 to 12 keV using the merged MOS1/2 data.

2.2. Spectral analysis

The energy spectrum of G296.7–0.9 was extracted from an elliptical annular sector with the center at RA_c and DEC_c , semi major axes of $5'$ and $2'.9$, semi minor axes of $3'.75$ and $2'.2$ and an opening angle of 140° . The background spectrum was derived from a nearby region placed on the same MOS1/2 chip with the same size as the source region. The background contribution was found to be $\approx 50\%$ in the two MOS cameras and $\approx 71\%$ in the PN data. After subtracting the background 1232, 1236, and 3077 source counts remained in the MOS1, MOS2, and PN data. For the spectral analysis of the remnant these counts were binned to have at least 75 counts per bin in the case of the MOS1/2 observations and 150 counts per bin for the PN data.

We checked whether the spectral fitting results will change, if we model the instrumental background according to the suggestions made by Kuntz & Snowden (2008). They proposed to add a Gaussian at the fluorescent line of Al $K\alpha$ at $E = 1.49$ keV with zero width and a power law model for modeling the remaining soft proton contamination. This power law model is not convolved with the instrumental response. As it turns out from this analysis the model fits were not significantly better than without adding these components using the standard F-test. Thus, the following results are without modeling the instrumental background separately.

We fitted the X-ray spectrum of G296.7–0.9 with various models: A hot diffuse gas model (MEKAL, $\chi^2 = 139.6$ for 95 d.o.f.), a model for a collisionally ionized diffuse gas (APEC, $\chi^2 = 107.0$ for 95 d.o.f.), a power law model ($\chi^2 = 235.3/95$ d.o.f.), a thermal bremsstrahlung model ($\chi^2 = 243.3$ for 95 d.o.f.), a Raymond-Smith diffuse gas model ($\chi^2 = 151.7/95$ d.o.f.), a non-equilibrium collisional plasma that allows a temperature evolution (GNEI, $\chi^2 = 88.6$ for 93 d.o.f.) or has a constant temperature (NEI, $\chi^2 = 89.3$ for 94 d.o.f.), a plane-parallel shock plasma model (PSHOCK, $\chi^2 = 87.5$ for 94 d.o.f.), an ionization equilibrium collisional plasma model (EQUIL, $\chi^2 = 96.8$ for 95 d.o.f.), and a Sedov model with separate ion and electron temperature ($\chi^2 = 90.0/93$ d.o.f.). For spectral models with $\chi^2_{red} < 1.4$, all fit parameters are listed in Table 2. The NEI model fit is shown in Figure 2.

In the following, we will use the best-fit results of the NEI model to derive related SNR parameters. For all models with a non-equilibrium equation of state we measure an ionization timescale value $\tau = t_0 N_e < 10^{12}$ s cm^{-3} (t_0 is the age of the remnant and N_e the post-shock electron number density), which is

¹ <http://vizier.u-strasbg.fr/viz-bin/VizieR>

² xmm.vilspa.esa.es/docs/documents/CAL-TN-0018.pdf.

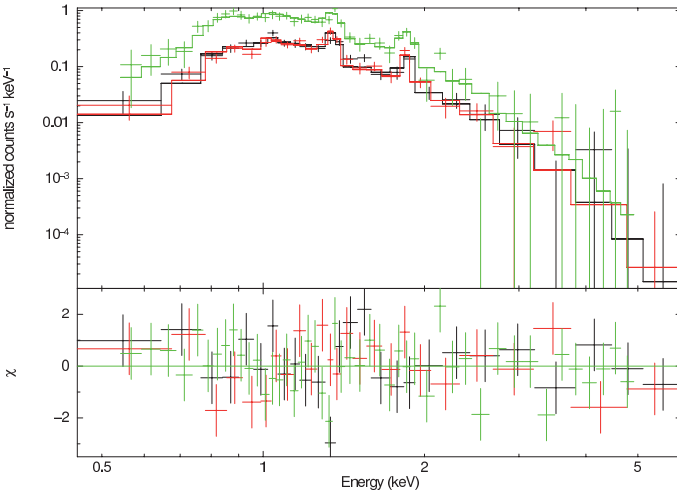
Table 1. Detected sources in XMM-Newton observation 0675070101. The sources are denoted as in Fig. 1.

Source	RA (J2000)	DEC (J2000)	δ RA/DEC	S/N	optical counterpart (positional discrepancy)
	h:m:s	d:m:s	arcsec	σ_G	
1	11:57:05.73	-63:04:52.8	2.3	7.7	2MASS J11570561-6304504 (2'5)
2	11:56:53.90	-63:05:13.1	2.1	8.5	USNO-B1.0 0269-0325437 (2'3)
3	11:55:28.64	-63:03:17.8	2.2	7.0	2MASS J11552811-6303136 (4'9)
4	11:54:51.16	-63:13:31.3	2.0	34.1	2MASS J11545063-6313269 (5'7)
5	11:54:31.06	-63:01:32.7	2.0	22.2	HD 103442 (4'0)

Table 2. Spectral parameters of the best-fit models for SNR G296.7–0.9.

model	n_H [10^{22} cm^{-2}]	$k_B T$ [keV]	τ^α [10^{11} s/cm^3]	$k_B T_e^\beta / \langle kT \rangle^\gamma$ [keV]	Norm $^\delta$ [10^{-2} cm^{-5}]	$\chi^2/\text{d.o.f.}$	f_X^ϵ [$10^{-11} \text{ erg cm}^{-2} \text{ s}^{-1}$]
NEI	$1.24^{+0.07}_{-0.05}$	$0.53^{+0.08}_{-0.07}$	$1.2^{+0.8}_{-0.4}$	-/-	$1.3^{+0.6}_{-0.3}$	89.3/94	$5.2^{+1.1}_{-0.9}$
PSHOCK	$1.16^{+0.14}_{-0.06}$	$0.54^{+0.08}_{-0.06}$	8^{+15}_{-7}	-/-	$1.1^{+0.6}_{-0.2}$	87.5/94	$3.5^{+0.5}_{-0.3}$
SEDOV	$1.27^{+0.10}_{-0.09}$	$0.35^{+0.19}_{-0.08}$	6^{+7}_{-4}	$< 0.54/-$	$2.3^{+2.1}_{-0.9}$	89.4/93	8 ± 3
GNEI	1.27 ± 0.08	$0.49^{+0.11}_{-0.08}$	$1.0^{+0.8}_{-0.5}$	$-/0.55^{+0.11}_{-0.08}$	$1.5^{+0.9}_{-0.6}$	88.6/93	$6.0^{+1.0}_{-1.5}$
EQUIL	1.10 ± 0.04	0.52 ± 0.04	-	-/-	$1.09^{+0.21}_{-0.15}$	96.8/95	2.5 ± 0.2
APEC	1.23 ± 0.05	$0.38^{+0.10}_{-0.03}$	-	-/-	$2.0^{+0.6}_{-0.5}$	107.0/95	$4.6^{+0.6}_{-0.5}$

Notes. $^{(\alpha)}$ ionization timescale $^{(\beta)}$ electron temperature immediately behind the shock front $^{(\gamma)}$ ionization timescale-averaged temperature $\langle kT \rangle = \int_{t_s}^0 T(t) N_e(t) dt / \tau$ $^{(\delta)}$ Norm = $\frac{10^{-14}}{4\pi[D_A(1+z)]^2} \int N_e N_H dV$, where D_A is the angular diameter distance to the source in cm, N_e and N_H are the post-shock electron and hydrogen densities in cm^{-3} , respectively. $^{(\epsilon)}$ X-ray flux in the energy range 0.5 to 4.0 keV.

**Fig. 2.** Spectrum and fitted model (NEI) of the X-ray emission of SNR G296.7–0.9. In black the MOS1, red the MOS2 and green the PN data.

smaller than the expected timescale at which collisional ionization equilibrium is reached (Borkowski et al. 2001). Therefore, the APEC and EQUIL model can be neglected. For the GNEI model the temperature and the ionization timescale-averaged temperature are almost the same, which is no improvement over the NEI model. Additionally, we will not use the results of the SEDOV model any further, because the determination of the postshock temperature T_e in that model is only possible at energies above 3 to 4 keV (Borkowski et al. 2001) where the spectrum of G296.7–0.9 is not well constrained.

The value for n_H in the NEI model fit is lower than the average integrated hydrogen column density toward SNR G296.7–0.9, which is $n_H^{LAB} = 1.39 \times 10^{22} \text{ cm}^{-2}$ (Kalberla et al. 2005). This value is based on HI emission line measurements at a ra-

dio frequency of 21 cm and refers to the entire hydrogen column density in the line of sight.

The temperature of the plasma is $6.2^{+0.9}_{-0.8} \times 10^6$ Kelvin and no significant deviation of the best-fit statistic was obtained when allowing the abundances to differ from the solar values. Using the derived parameters of the NEI model fit the flux in the 0.5 to 4 keV band is $5.2^{+1.1}_{-0.9} \times 10^{-11} \text{ erg/cm}^2/\text{s}$.

In addition we investigated the spatial variation of the spectral parameters by extracting all photons in the northern and southern part of the remnant. However, no difference can be assessed within the derived errors.

3. Discussion

3.1. Comparison with the ROSAT results

Schaudel (2003) and Robbins et al. (2012) analyzed two pointed ROSAT PSPCB observations independently of each other. These data were taken between 1st and 8th of February 1993 and 19th and 21st of February 1998. Both authors found a temperature of the X-ray emitting gas and a hydrogen column density n_H toward the source that is lower by at least a factor of two when compared with the results deduced in our work. Only Schaudel (2003) found an n_H that is comparable with our value listed in Table 2 by fitting the Raymond-Smith model, though his value had a much higher uncertainty. As already mentioned in the introduction, the PSPCB had about five independent energy channels, which limits the conclusions drawn from their spectral fittings, especially when 70 spectral bins were used as in the work of Robbins et al. (2012). This corresponds to an oversampling of about 15 times the spectral resolution of the detector!

3.2. Supernova remnant

Using the deduced spectral parameters from the NEI fit we can derive basic properties of the remnant, such as the distance d ,

post-shock hydrogen density N_H , sweep-up mass M , the age of the remnant t , the radius in pc R_s , and the shock velocity v_s .

We used the following set of equations, which is described in detail in Prinz & Becker (2012, and references therein).

$$\begin{aligned} d_{\text{Sedov}} &= 7420 \cdot \theta^{-3/5} \left(\frac{E_{51}}{T_s} \right)^{2/5} \left(\frac{f}{\text{Norm}} \right)^{1/5} [\text{kpc}] \\ d_{\text{Reddening}} &= n_H / (n_H / A_V \cdot A_V / E_{B-V} \cdot E_{B-V} / \text{kpc}) [\text{kpc}] \\ V_{\text{emit}} &= 3.029 \times 10^{54} \cdot f \cdot \theta^3 \cdot (d_{\text{Sedov}} [\text{kpc}])^3 [\text{cm}^3] \\ N_H &= 70.27 \sqrt{\frac{\text{Norm}}{d_{\text{Sedov}} \cdot f \cdot \theta^3}} [\text{cm}^{-3}] \\ M &= 1.4 \cdot N_H \cdot m_H \cdot V [\text{kg}] \\ t &= 2.71 \times 10^9 \left(\frac{E_{51}}{N_H} \right)^{1/3} T_s^{-6/5} [\text{yr}] \\ R_s &= 0.34 \left(\frac{E_{51}}{N_H} \right)^{1/5} t^{2/5} [\text{pc}] \\ v_s &= \frac{2}{5} \frac{R_s}{t} [\text{km/s}]. \end{aligned}$$

Herein $\theta = \sqrt{\text{major} \times \text{minor axis}}$ is the reduced radius of the remnant in arcmin, E_{51} the explosion energy in units of 10^{51} erg, T_s the fitted plasma temperature, f the filling factor to correct for the morphology of the SNR, Norm the normalization of the spectral fit, n_H the fitted hydrogen column density, V_{emit} is the X-ray emitting volume, and m_H the mass of a hydrogen atom.

From the distribution of mean color excess E_{B-V} per kiloparsec derived by Lucke (1978) we found $E_{B-V}/\text{kpc} = 0.25 \pm 0.10$ in the direction of the remnant. In addition, we used the relation between n_H and the visual extinction A_V of Predehl & Schmitt (1995) $n_H/A_V = (1.79 \pm 0.03) \times 10^{21} \text{ cm}^{-2}$ and the relation between A_V and the color excess $A_V/E_{B-V} = 3.2 \pm 0.2$ (Zombeck 2007). This leads to a distance of $d_{\text{Reddening}} = 9 \pm 4 \text{ kpc}$.

The Sedov-analysis based distance is $d_{\text{Sedov}} = 9.8^{+1.1}_{-0.7} \text{ kpc}$. In the following, we give all important quantities in units of $d_{9.8} = d/9.8 \text{ kpc}$ as d_{Sedov} has a smaller uncertainty than other distance estimates. Furthermore, the mean color excess $\langle E_{B-V} \rangle$ which we used to calculate $d_{\text{Reddening}}$ was derived for a reddening layer up to 2 kpc and thus is just a rough estimate. From Figure 1 we infer that only $f = 15\%$ of the remnant is bright enough to be used for spectral analysis. Therefore, the post-shock hydrogen density N_H is $0.73^{+0.18}_{-0.10}$ and the sweep-up mass is $M = 29 M_\odot d_{9.8}^{5/2}$. Assuming that the explosion energy E is equal to the canonical value of 10^{51} erg, the age of the remnant is 5800 to 7600 years and the radius is $R_s = 12.2^{+1.2}_{-0.8} d_{9.8}^{1/6} \text{ pc}$. We derive a shock velocity v_s of $720^{+130}_{-100} \text{ km/s}$. Using the flux values deduced in Section 2 we compute its luminosity to be $L_X^{0.5-4} = 6.0^{+1.8}_{-1.4} \times 10^{35} d_{9.8}^2 \text{ erg/s}$.

3.3. Compact central object

To obtain a rough estimate of the flux upper limit for a hypothetical compact source in the center of the remnant, we assumed that the source is CCO-like. No compact source nor a radio pulsar has been detected in G296.7–0.9 so far (Robbins et al. 2012). Like other CCOs, e.g. the one in the SNR Puppis A, we assume that the spectrum is dominated by blackbody emission with a temperature of $\approx 2.6 \times 10^6$ Kelvin and a luminosity in the 0.5–10 keV band of at least 10^{32} erg/s (see Becker 2009, for a review). This corresponds to a flux in this energy range of $\approx 9 \times 10^{-15}$

$\text{erg cm}^{-2} \text{ s}^{-1}$. Using the WebPIMMS tool with the fitted n_H of the SNR the count rate in the 0.2–12 keV range is $> 4 \times 10^{-4} \text{ cts/s}$ for the merged MOS1 and MOS2 observations, an order of magnitude lower than the derived 3σ upper limit for a point-like source at the center of the remnant.

4. Conclusion and summary

The remnant is characterized by a bright arc in the south-west direction and by diffuse emission with low surface brightness in its western part. We showed that the X-ray emission of G296.7–0.9 is in agreement with coming from a collisionally heated plasma which has not reached equilibrium yet. The Sedov analysis lead to the conclusion that the SNR is about 6600 years old and is expanding with a velocity on the order of $\approx 720 \text{ km/s}$.

The close-by HII region G296.593–0.975 has a velocity of $+25 \pm 1 \text{ km s}^{-1}$ based on measured hydrogen recombination lines (Caswell & Haynes 1987). With the standard IAU parameter for the distance to the center of our Galaxy $R_0 = 8.5 \text{ kpc}$ and the solar orbit velocity of $V_0 = 220 \text{ km/s}$ derived by Kerr & Lynden-Bell (1986) and the Galactic rotation model of Fich et al. (1989) we deduce a distance to the HII region of $9.3 \pm 0.6 \text{ kpc}$. For the error estimate we assumed an uncertainty in the velocity-to-distance conversion of 7 km/s (e.g., Clifton et al. 1988).

The deduced distance d_{Sedov} is in perfect agreement with the distance of the close-by HII region G296.593–0.975. This is a strong indicator for a spatial connection between the SNR and the HII region as already suggested by Robbins et al. (2012).

The used XMM-Newton observation was strongly affected by radiation, which lead to a net observation time that was shorter by a factor of three than the approved exposure time. Therefore, only limited statements can be made about the existence of a compact source located near the center of the supernova remnant. Deeper observations are needed to clarify this question in more detail.

Acknowledgements. We acknowledge the use of the XMM-Newton data archive. T.P. acknowledges support from and participation in the International Max-Planck Research School on Astrophysics at the Ludwig-Maximilians University.

References

- Becker, W. 2009, in *Astrophysics and Space Science Library*, Vol. 357, Astrophysics and Space Science Library, ed. W. Becker, 91
- Borkowski, K. J., Lyerly, W. J., & Reynolds, S. P. 2001, *ApJ*, 548, 820
- Caswell, J. L. & Haynes, R. F. 1987, *A&A*, 171, 261
- Clifton, T. R., Frail, D. A., Kulkarni, S. R., & Weisberg, J. M. 1988, *ApJ*, 333, 332
- Fich, M., Blitz, L., & Stark, A. A. 1989, *ApJ*, 342, 272
- Green, D. A. & Stephenson, F. R. 2003, in *Lecture Notes in Physics*, Berlin Springer Verlag, Vol. 598, *Supernovae and Gamma-Ray Bursters*, ed. K. Weiler, 7–19
- Kalberla, P. M. W., Burton, W. B., Hartmann, D., et al. 2005, *A&A*, 440, 775
- Keane, E. F. & Kramer, M. 2008, *MNRAS*, 391, 2009
- Kerr, F. J. & Lynden-Bell, D. 1986, *MNRAS*, 221, 1023
- Kuntz, K. D. & Snowden, S. L. 2008, *A&A*, 478, 575
- Lucke, P. B. 1978, *A&A*, 64, 367
- Predehl, P. & Schmitt, J. H. M. M. 1995, *A&A*, 293, 889
- Prinz, T. & Becker, W. 2012, *A&A*, 544, A7
- Rest, A., Welch, D. L., Suntzeff, N. B., et al. 2008, *ApJ*, 681, L81
- Reynolds, S. P., Borkowski, K. J., Green, D. A., et al. 2008, *ApJ*, 680, L41
- Robbins, W. J., Gaensler, B. M., Murphy, T., Reeves, S., & Green, A. J. 2012, *MNRAS*, 419, 2623
- Rodney, S. A., Riess, A. G., Strolger, L., et al. 2011, in *American Astronomical Society Meeting Abstracts* #218, #219.01
- Sako, M., Bassett, B., Becker, A., et al. 2008, *AJ*, 135, 348
- Schudel, D. 2003, PhD thesis, LMU, Germany

- Schaudel, D., Becker, W., Voges, W., et al. 2002, in Astronomical Society of the Pacific Conference Series, Vol. 271, Neutron Stars in Supernova Remnants, ed. P. O. Slane & B. M. Gaensler, 391
- Strüder, L., Briel, U., Dennerl, K., et al. 2001, A&A, 365, L18
- Zombeck, M. 2007, Handbook of Space Astronomy and Astrophysics: Third Edition, ed. Zombeck, M. (Cambridge University Press)